Applied Surface Science 540 (2021) 148309

Contents lists available at ScienceDirect

Applied Surface Science

journal homepage: www.elsevier.com/locate/apsusc

# Thermal gas-phase etching of titanium nitride (TiN) by thionyl chloride ($SOCl_2$)

Varun Sharma [a,b,*], Tom Blomberg [a,c], Suvi Haukka [a], Shaun Cembella [d], Michael E. Givens [a], Marko Tuominen [a], Rajesh Odedra [d], Wes Graff [d], Mikko Ritala [b]

[a] ASM Microchemistry Oy, Pietari Kalmin katu 3 F2, 00560 Helsinki, Finland
[b] Department of Chemistry, University of Helsinki, FI-00014 Helsinki, Finland
[c] Department of Chemistry and Materials Science, Aalto University, 02150 Espoo, Finland
[d] Seastar Chemicals ULC, 2061 Henry Ave W, Sidney, BC V8L 5Z6, Canada

ARTICLE INFO

*Keywords:*
Dry etching
Thermal etching
Titanium nitride
Thionyl chloride
Selective etching

*2010 MSC:*
00-01
99-00

ABSTRACT

In this work, thermal based gas-phase etching of titanium nitride (TiN) is demonstrated using thionyl chloride ($SOCl_2$) as a novel etchant. A single etchant is utilised in a pulsed fashion to etch TiN. This type of etching technique may also be considered as a chemical gas-phase or dry etching. The removed TiN amount was measured by various techniques like spectroscopic ellipsometry (SE), weighing balance and in some cases X-ray reflectometry (XRR). Additionally, the post-etch surfaces were analysed with X-ray photoelectron spectroscopy (XPS) and bright field transmission electron microscopy (BF-TEM). The surface roughness and morphology of before and after etching TiN films were measured using atomic force microscopy (AFM). The etch per cycle (EPC) was calculated and is plotted as a function of $SOCl_2$ pulse time, purge time after $SOCl_2$ exposure, number of etch cycles and etch temperature ($T_{etch}$). An increase in EPC with an increase in $SOCl_2$ pulse time as well as etch temperature was observed. $SOCl_2$ is able to etch TiN starting from 270 °C with an EPC of about 0.03 Å to almost 1.2 Å at 370 °C. Arrhenius plot determined the activation energy ($E_a$) of about 25 kcal/mol for TiN etching by $SOCl_2$. In addition, the etch selectivity between different substrates such as silicon dioxide ($SiO_2$), silicon nitride ($Si_3N_4$) and aluminum oxide ($Al_2O_3$) was investigated on blanket as well as 3D structures. Moreover, thermodynamic calculations were performed for various possible etch reactions. Titanium from TiN is proposed to be etched in the form of either titanium trichloride ($TiCl_3$) or titanium tetrachloride ($TiCl_4$). Nitrogen from TiN films may form volatile by-products such as diatomic nitrogen ($N_2$), nitrous oxide ($N_2O$) and nitrogen dioxide ($NO_2$).

## 1. Introduction

Removing material from the surface has been one of the key steps in fabricating complex semiconductor as well as micromachining of MEMS devices [1] and several etch techniques have been employed in order to realize this. In thin-film technology the most widely used etch techniques both in academia as well as industry are either based on liquid phase, plasma [2], gas-phase [1,3,4] or recently explored atomic layer etching by thermal means [5]. In today's era of nano-devices, atomic-level processing requires extreme precision with high accuracy to maintain the device performance and reliability. These criteria can be fulfilled by techniques that allow thickness control within a few angstroms and are atomic layer deposition [6,7], plasma based atomic layer etching (ALE) or quasi-ALE [2,8], thermal ALE [5] and gas-phase pulsed etching techniques.

In this paper we explore potential of chemical based gas-phase pulsed etching (GPPE) and its capability to etch material with angstrom-level thickness control. A gas-phase etching may involve a single etchant and can be either continuous or pulsed etching[3]. One advantage of GPPE over continuous etching is that it provides etch cycles as an additional knob to digitally control the etched amount, and thus removed thickness. Ideally in a GPPE technique, an etched thickness is a linear function of etch cycles. In addition, choice of optimal process parameters may provide etching in the angstrom per cycle regime.

In the semiconductor industry, isotropic gas-phase etching has been known since the mid 60s and was first studied by Holmes and Snell [9]. They discovered an etching of silicon dioxide ($SiO_2$) by hydrogen

* Corresponding author at: ASM Microchemistry Oy, Pietari Kalmin katu 3 F2, 00560 Helsinki, Finland.
*E-mail addresses:* Varun.Sharma@helsinki.fi (V. Sharma), Mikko.Ritala@helsinki.fi (M. Ritala).

https://doi.org/10.1016/j.apsusc.2020.148309
Received 3 July 2020; Received in revised form 7 October 2020; Accepted 27 October 2020
Available online 4 November 2020

fluoride (HF) vapors [1]. Later several gas-phase etch systems were developed and thoroughly studied by many investigators, a few examples of such etch systems are silicon etch by xenon difluoride ($XeF_2$) [10], boron trifluoride ($BF_3$) [10], hydrochloric acid (HCl) vapors [11], inter-halogen compounds [12], and $SiO_2$ vapor phase removal by HF-alcohol mixtures[3,4,13]. $XeF_2$ is also known to show selective etching of silicon at low temperatures with no significant etching of $SiO_2$, silicon nitiride $Si_3N_4$, silicon carbide (SiC), metals, dielectrics and polymers observed [14,12,1]. On the other hand, HF vapors were able to etch native oxide selectively over silicon [15]. Apart from silicon based materials, carbon and polymer films were shown to be etched by ozone gas near room temperature. [16] This is a typical example of combustion or ashing reactions. Zhang et al. showed etching of carbon nano-tubes by gas-phase plasma hydrocarbonation reactions[13] and this particular chemistry was able to etch metallic carbon nanotubes selectively while retaining semiconducting carbon nanotubes. In addition many plasma based etch processes for metal nitrides such as crystalline aluminum nitride (AlN), titanium nitride (TiN)[17], and III-V nitrides[18] are well established [19–21]. However, most plasma etch processes involve energetic species such as ions, radicals and UV-VUV photons[22,23] that are known to induce surface damage and deteriorate the post-etch film properties[24] and have high etch rates[25,18,26]. Furthermore the fluorine or chlorine based plasma etch processes may provide limited selectivity and leave surface contaminated, especially when considering other materials such as $SiO_2$, Si, $Si_3N_4$ and $Al_2O_3$ on the wafer surface, simultaneously [27,18,17,28,29].

So far, TiN has been thermally etched by first oxidizing TiN to $TiO_2$ and then utilizing HF vapors to remove the converted $TiO_2$ layer and repeating the cycle as needed[30]. In contrast, no thermal gas-phase cyclic etching processes for TiN without any oxidation step has been reported. Such etching process for TiN can be useful in various applications in the semiconductor industry; for instance, controlled thinning of metal liners, tuning of threshold gate voltage[28], isotropic etching of hard masks[29], improving conformality of diffusion barriers as well as ohmic metal electrodes, and anti-reflective[26] coatings etc.

In this paper, we study novel chemical dry etch process for the etching TiN selectively over $SiO_2$, $Si_3N_4$ and $Al_2O_3$. $SOCl_2$ was chosen as an etchant to avoid any extra oxidation step as well as surface contaminations, mitigate any plasma induced damage[17], develop fluorine free process, etch from non line-of-sight features, enhance the etch-selectivity, and provide angstrom-level thickness control when applied in pulsed fashion.

## 2. Experiment

### 2.1. Etch-targets and process gases

All etching experiments were performed on p-type 200 mm silicon wafers and selected etch-target materials were $SiO_2$, $Si_3N_4$, $Al_2O_3$ and TiN. The $SiO_2$ used in the etch experiments was either thermally grown oxide of about 20 nm in thickness or 15 nm $SiO_2$ grown by plasma-enhanced atomic layer deposition (PEALD) technique[31]. The $Si_3N_4$ was 20 nm thick high quality low pressure chemical vapor deposited (LPCVD) nitride. $Al_2O_3$ of about 20 nm was deposited at 300 °C by trimethylaluminum (TMA) and water ($H_2O$) based ALD process[32]. TiN was deposited on 20 nm thermal oxide at 400 °C by thermal ALD process utilizing $TiCl_4$ and $NH_3$[33]. TiN films were from 10 to 50 nm. The expected thickness of TiN grown without an air break was around 15 nm and 20 nm.

The $SOCl_2$ as an etchant was purchased from Seastar Chemicals Inc (Canada), with high purity (> 99.9999 %) and ultra low metal contaminations (< 1 ppb). It was kept at room temperature as it has sufficiently high vapor pressure of about 93 Torr at 293 K. [34] Due to its high vapor pressure, $SOCl_2$ was used in vapor-draw mode, $N_2$ was utilised as a purge gas. Both $N_2$ purge gas flow as well as the $SOCl_2$ dose were controlled by needle valves. The facility gas $N_2$ used in the etch processes was 99.999 % (5.0) pure and further purified by an Entegris purifier to ⩾99.9999 % purity (6.0) level.

### 2.2. Experimental setup and methodology

All etch experiments were performed in a commercial ASM Pulsar ® 2000 (P2000) reaction chamber with automatic wafer handling system. The P2000 chamber has an inner reaction chamber that is isolated inside an outer vacuum chamber. The reactor was operated at isothermal conditions to a maximum $T_{etch}$ of 370 °C and the pressure varied roughly between 1 and 3 Torr. A thick coating of corrosive resistant material was deposited on the inner walls of reaction chamber prior to etch experiments. All the TiN coated wafers subjected to etch experiments were kept in the chamber for 5 minutes prior to etch to ensure wafer temperature stabilization.

The etch per cycle (EPC) was estimated by measuring the post-etch thickness and subtracting it from the pre-etch thickness values by spectroscopic ellipsometry (SE) and dividing by total number of etch cycles. For comparison reasons, the exact center point of the wafers were measured by SE. In addition, the thickness and EPC values for TiN films were extracted from the weight measurements. The substrates were weighed before as well as after etching. The obtained change in mass was used to calculate the removed thickness of TiN films by using simple mass-density-volume relationship[35]. This technique was adopted in order to characterize etch process as it worked reliably better for thicker as well as thinner films. Due to the nature of this methodology of pre and post-etch measurements, the oxidation of TiN films in air became inevitable. Thus, TiN films were probably oxidized in air before and after etching unless otherwise stated. In some cases, XRR was also used to confirm the thickness and extract density values of TiN films. No significant discrepancies were found between thickness measurements from SE, weight and XRR techniques as shown below. For simplicity, the thickness and EPC values reported here are extracted from weight measurements except in Fig. 5.

### 2.3. Characterization techniques and equipment

The model of a balance used to weigh the amount of removed material was SAG 204 from Mettler Toledo. This particular model has a resolution of about 0.1 mg with a stabilization time more than 3 s.

The ellipsometer used to measure thickness and optical constants of various films was SE 800 from Sentech. The density and thickness verification was performed by using PANalytical Xpert PRO MRD X-ray diffractometer.

A fully integrated XPS system from Thermo Scientific™ K-Alpha$^+$ was used to verify the film composition and perform surface analysis. This specific system is equipped with a 180° double focusing hemispherical analyzer with 128 channel detector. A monochromatic Al K$\alpha$ X-ray source (1486.6 eV) was used to collect a survey as well as high resolution scans for individual elements. For a survey scan the pass energy of 200 eV and a step size of 1 eV was used. The high resolution elemental scans were collected with pass energy of 30 eV and a step size of 0.1 eV. An X-ray spot size was about 400 µm. This particular XPS system is also fitted with a dual beam flood gun for any charge compensation. The Avantage® v5.962 software package was employed to collect and analyze the data. XPS detection limit is around 0.1 at.% and fitting error is estimated to be around 0.5 at.%. The error in binding energies is evaluated to be ±0.1 eV. All the peaks were calibrated to the adventitious C 1s peak centered at 284.8 eV

TEM analysis was performed by Evans Analytical Group (EAG), California. The samples for TEM were prepared using the in situ focused ion beam (FIB) lift-out technique on an FEI Dual Beam FIB/SEM. For contrast and preserving the sample structural integrity, carbon coating was performed followed by sputtering of Ir and Pt on top prior to ion-milling. The TEM lamella thickness was about 100 nm and the samples were imaged with a FEI Tecnai TF-20 FEG/TEM operated at 200 kV

in bright-field TEM modes.

For AFM imaging, the Bruker Dimension HPI tool operated by Nanoscope software 9.4 was used. The images were captured using ScanAsyst® tapping mode. The processing of high resolution images was carried out on a Nanoscope Analysis 2.0 software. The image resolution was set to 500 nm × 500 nm.

The thermodynamics of the solid–gas reactions were calculated using HSC Chemistry 4.1 software from Outotec.

## 3. Results and Discussion

### 3.1. Thermodynamic calculations

The feasibility of using $SOCl_2$ as an etchant for selected materials was first assessed by thermodynamic calculations. Therefore a change in the Gibbs free energy (ΔG) as well as a change in enthalpy (ΔH) were calculated from HSC for several possible reactions between gaseous $SOCl_2$ and various film materials. All reactions discussed under this section do have a positive change in entropy at all temperatures.

The film materials such as TiN, $Al_2O_3$, $SiO_2$ and $Si_3N_4$ were chosen from HSC library in the form of solid for a close representation of the thin-films. The choice of by-products was limited to the species that are either volatile or available in the gaseous form. Various by-products that were chosen in gaseous phase are aluminum trichloride ($AlCl_3$), aluminum oxychloride (AlOCl) [36], silicon tetrachloride ($SiCl_4$), titanium oxydichloride ($TiOCl_2$), titanium oxymonochloride (TiOCl), titanium trichloride ($TiCl_3$), titanium tetrachloride ($TiCl_4$), oxygen ($O_2$), nitrogen ($N_2$), nitrous oxide ($N_2O$), nitrogen dioxide ($NO_2$), sulfur dioxide ($SO_2$), sulfur mono-oxide (SO) and disulfur dichloride ($S_2Cl_2$). From this finite list of reactants and by-products, several possible overall reactions were considered and the reactions with their corresponding ΔG values at different temperatures are plotted in Fig. 1 and Fig. 2. Some overall reactions were discarded due to several reasons such as very high positive ΔG throughout the temperature range, balancing issues or by-products with low volatility (e.g. TiOCl) and are not shown here.

Fig. 1 plots a change in Gibbs free energy at various temperatures for TiN. A majority of the reactions between TiN and $SOCl_2$(g) did show negative change in Gibbs free energy. This also corroborates our experimental findings below. From the reactions described in Fig. 1,

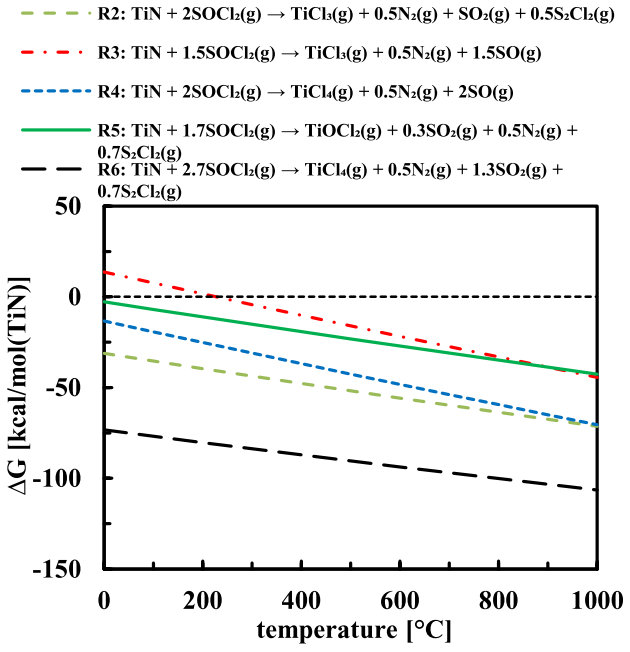


**Fig. 1.** A change in Gibbs free energy at different temperatures for various possible chemical reactions between TiN and $SOCl_2$(g).

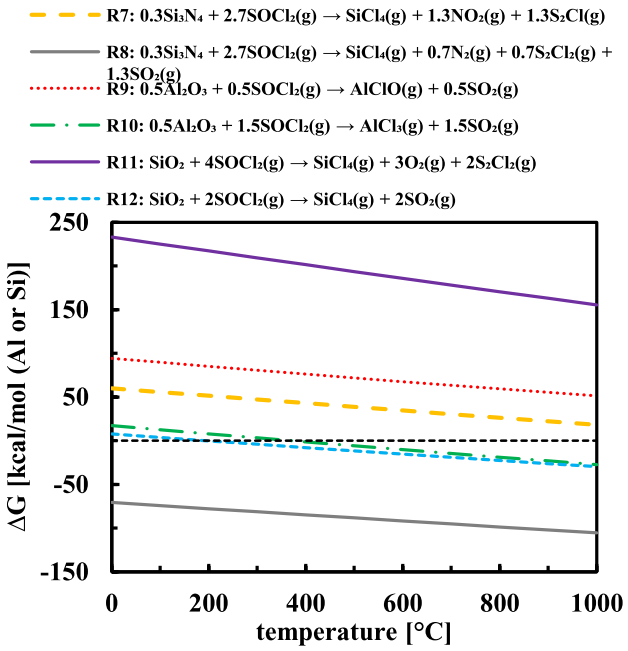


**Fig. 2.** A change in Gibbs free energy vs temperatures for few possible chemical bulk reactions between reactants like $SiO_2$, $Si_3N_4$ or $Al_2O_3$ and $SOCl_2$(g).

possible volatile by-products that can be formed in the etching process of TiN are $TiCl_4$(g), $TiCl_3$(g) and $TiOCl_2$(g). A nitrogen from the TiN films can form stable volatile by-products for example diatomic nitrogen, nitrogen dioxide and nitrous oxide. For example, a chemical reaction with negative change in Gibbs free energy where $N_2O$ can be considered as a by-product is described by **R1** below. On the other hand, sulfur can also undergo a change in its oxidation state and therefore by-products like $SO_2$(g), SO(g) and $S_2Cl_2$(g) are clearly plausible as evident from reactions **R1** to **R6**. In Fig. 1, only **R2** and **R6** are exothermic (i.e. ΔH < 0) and others are endothermic at all temperatures.

$$\mathbf{R1}: TiN + 2.9SOCl_{2(g)} -> TiCl_{4(g)} + 0.5N_2O_{(g)} + 1.2SO_{2(g)} + 0.9S_2Cl_{2(g)} \quad (1)$$

Fig. 2 shows a change in Gibbs free energy as a function of temperature for some possible reactions between film materials such as $SiO_2$, $Si_3N_4$, and $Al_2O_3$ and $SOCl_2$(g) as an etchant. Almost all chemical reactions except **R8** in Fig. 2, are endothermic due to positive change in enthalpy at all temperatures (≲1000 °C).

For a successful etching of $Al_2O_3$ by $SOCl_2$(g), aluminum must form compounds with chlorine which are volatile within the tested etch temperature regime and are $AlCl_3$ as well as its dimer form $Al_2Cl_6$ [37]. However, a possibility of AlOCl(g) as a by-product can be neglected due to a very high positive change in Gibbs free energy as shown by **R9** in Fig. 2. Moreover, similar conclusion about AlOCl(g) was made by Greenbaum[36] and Harald[38] from their experimental results as well as thermodynamic calculations. From Fig. 2, it can be concluded that thionyl chloride alone is unable to etch $Al_2O_3$ and thus supports our experimental findings shown below.

A reaction **R12** in Fig. 2, between $SiO_2$ and $SOCl_2$ has slightly negative change in Gibbs free energy above 200 °C but the change in enthalpy is positive (≳15 kcal) for the whole temperature range. This points toward an entropy driven, spontaneous reaction above temperatures of 200 °C. In case of $Si_3N_4$, only one reaction, i.e., reaction **R8** as shown in Fig. 2, is favorable (ΔH < 0) as well as spontaneous at all temperatures. However, our experiments did not show etching of $Si_3N_4$ or $SiO_2$ by $SOCl_2$(g) for temperatures between 270 °C and 370 °C. This can be explained by a reaction with slow kinetics or non-favourable surface-gas reactions.

### 3.2. Etching characteristics

Single etchant gas-phase etching of TiN films was performed by cyclic exposure to thionyl chloride ($SOCl_2$). Inert $N_2$ gas purges were introduced between the $SOCl_2$ pulses to ensure the proper removal of the by-products and excess $SOCl_2$ molecules from the etch system. The main purpose of the experiments below was to carry out the concept and feasibility studies for TiN etching by $SOCl_2$ and show selective removal of TiN over $SiO_2$, $Si_3N_4$ and $Al_2O_3$.

In Fig. 3, the etched thickness as well as etch per cycle as a function of $SOCl_2$ pulse time are shown. This series of experiments was performed at 320 °C etch temperature. A non-self limiting EPC response is observed upon increasing the $SOCl_2$ pulse time from 0 to 3 s. Low EPC of about 0.02 Å is determined at 0.5 s $SOCl_2$ pulse time and EPC increases quite linearly to about 0.36 Å for 3 s long thionyl chloride pulse time. After performing 1000 cycles of 3 s long $SOCl_2$ pulses, about 35 nm TiN film was removed as confirmed by various techniques like SE, weight measurements, XPS and XRR. The increase in etch per cycle is expected to continue with longer thionyl chloride pulse times. Furthermore, an EPC is expected to be a function of $SOCl_2$ partial pressures. Therefore in future it can be studied as well.

Fig. 4 captures the effect of purge time after 2 s $SOCl_2$ pulses on etch per cycle at 320 °C. An EPC of 0.16 Å is obtained for 2 s purge time and increased to 0.19 Å when 3 s $N_2$ purge time was applied. A significant increase in EPC from 0.19 Å to 0.55 Å was noticed at 8 s long purge time. This effect of an increase in EPC with an increase in purge time can be assigned to various factors like longer time for the source recovery and thus higher $SOCl_2$ dose, inefficient purging of $SOCl_2$ from the reaction chamber or delivery components especially from the gas lines that were kept at room temperature. Another factor that may contribute to this effect is the purge time required to remove less volatile species formed on TiN surface during the etch at 320 °C. The species that have lower volatility as compared to $TiCl_4$ are $TiCl_3$ [39] and $TiOCl_2$. Moreover, $TiCl_3$ is known to undergo a slow disproportionation reaction[40,41,39] according to **R12:** $2\,TiCl_3 \rightarrow TiCl_{2(s)} + TiCl_{4(g)}$. Hence, it is proposed that the formed $TiCl_3$ on the surface may partially get converted into more volatile $TiCl_4$ species thus leading to removal of titanium even during an inert purge step. Another possible reason for the increase in EPC with purge time is due to the presence of residual finite partial pressure of $SOCl_2$ in the chamber and thus a continuous slow etching. However, in the absence of data points at $N_2$ purge times higher than 8 s, it is difficult to say whether 8 s long $N_2$ purge time is sufficient or not to either completely remove the by-products or the etchant from the etch system. However, the EPC stayed below angstrom level and therefore the process allows good control on etched-thickness.

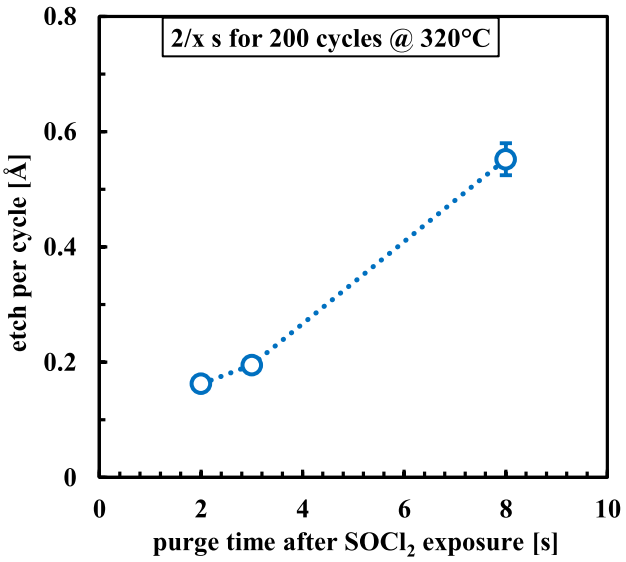


**Fig. 4.** Etch per cycle vs purge time after 2 s of $SOCl_2$ exposure at 320 °C for 200 cycles per data point.

In Fig. 5, the etched TiN thickness is plotted against total number of etch cycles for 2 s $SOCl_2$ pulse time with 3 s $N_2$ purges in-between. The etch temperature was kept constant at 320 °C. The figure shows a little difference in etched thickness is observed between oxidized and unoxidized TiN as well as slight difference due to the metrology employed. However, the coefficient of determination for the fitted line models varied between 0.96 and 0.98 and the derived constant EPC varied from 0.18 to 0.20 Å/cycle. After 1000 cycles of 2 s long $SOCl_2$ pulses, about 20 nm TiN film was completely removed and was also confirmed by XPS as seen below.

### 3.3. Etch selectivity

Various applications in thin-film technology require ability to etch one material over another selectively. Keeping this in mind, materials

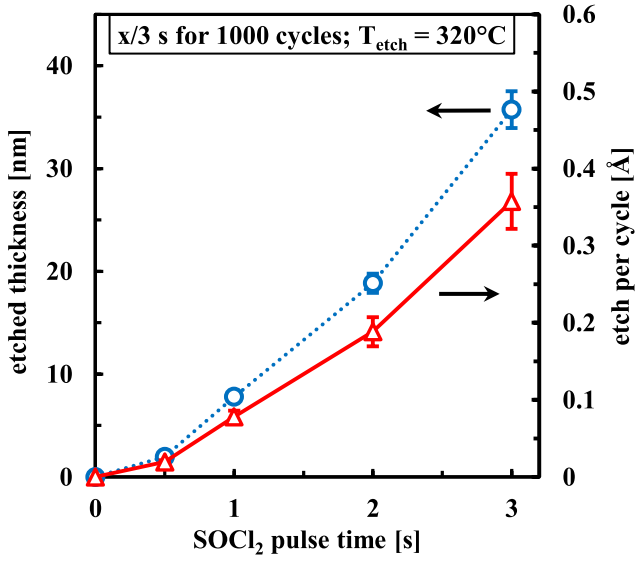


**Fig. 3.** Etched thickness (left axis) and corresponding etch per cycle (right axis) of TiN films vs $SOCl_2$ pulse time at 320 °C with 3 s of $N_2$ purges in-between.

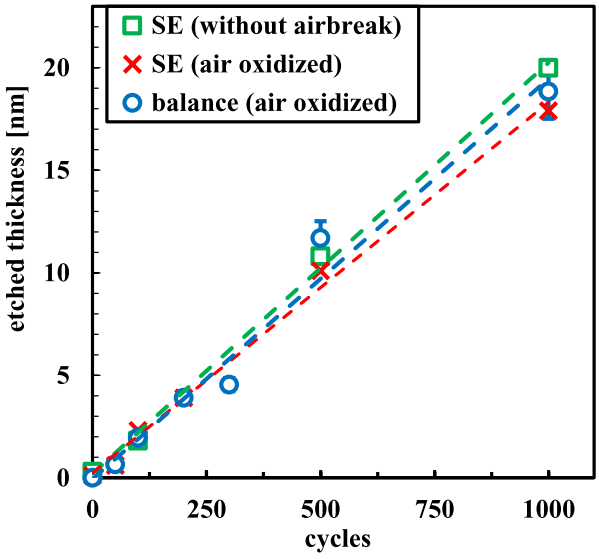


**Fig. 5.** Etched thickness vs total number of etch cycles at 320 °C for 2 s $SOCl_2$ pulse and 3 s $N_2$ purge is plotted.

like $Al_2O_3$, $SiO_2$ and $Si_3N_4$ were subjected to the same etch tests. Fig. 6 investigates the effect of etch temperature on various thin-film materials. From the figure it is clear that at higher etch temperatures, an increase in etch per cycle for TiN is observed. At etch temperatures below 270 °C, no significant TiN etching is observed for given settings for thionyl chloride dose. At 370 °C, EPC of about 1.2 Å is observed. No change in thickness was observed for $Al_2O_3$, $SiO_2$ and $Si_3N_4$ even after exposing to $SOCl_2$ for 1000 cycles. In other words, between 270 and 370 °C TiN can be etched by $SOCl_2$ selectively over $Al_2O_3$, $SiO_2$ and $Si_3N_4$. Moreover, a few experiments revealed that $SOCl_2$ is also able to etch PVD, CVD as well as PEALD grown TiN along with ALD deposited TiN. Higher etch temperatures (> 370 °C) can be also tested in future along with various test subjects such as other oxides, nitrides or carbides as well as pure metals of elements like Ti, W, Ta, Mo, Hf and Nb etc.

As shown in Fig. 7 the temperature dependence of the TiN etch per cycle within the temperature regime of 270 to 370 °C is investigated using an Arrhenius diagram, similar to the literature[42]. The same data points as in Fig. 5 are utilised. From the figure, it is clear that the logarithm of EPC varies linearly with the inverse of temperature. A linear-fit model (solid black line) with the high coefficient of determination ($R^2$ = 99.65) indicates a good agreement between predicted line and actual values (red points). The shaded area specifies 95% confident interval for the predicted line. From this plot, an activation energy $E_a$ of 24.7 kcal/mol is determined for the gas-phase pulsed etching of TiN by 2 s $SOCl_2$ pulses with 3 s in-between $N_2$ purges.

### 3.4. Post-etch analysis

After removing completely 20 nm TiN films from the thermally grown $SiO_2$ surface, it became important to study the surface remnants from the etch process. It is desirable to have very low surface contamination arising from the etch process itself. Therefore, XPS depth profiling measurements were done and the atomic percentages are plotted in Fig. 8 as a function of sputtering time. Fig. 8 suggests that the surface is mostly composed of silicon, oxygen and some surface carbon, with very low amounts of constituents from the etched titanium nitride films. A zoomed-in part of the figure reveals about 1.3 and 0.7 atomic percentages of nitrogen and titanium, respectively. A very small amount of chlorine, i.e., less than 0.5 atomic % was observed but no signal from sulfur was detected on any sample. These low amounts of surface remnants can be associated with incomplete etching and are anticipated to

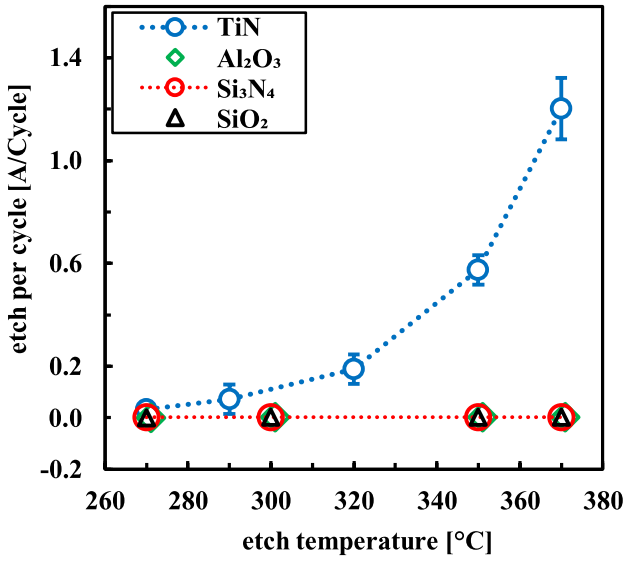


**Fig. 6.** Etch per cycle for TiN, $SiO_2$, $Al_2O_3$ and $Si_3N_4$ is plotted as a function of etch temperature. The $SOCl_2$ pulse and $N_2$ purge times were 2 and 3 s, respectively.

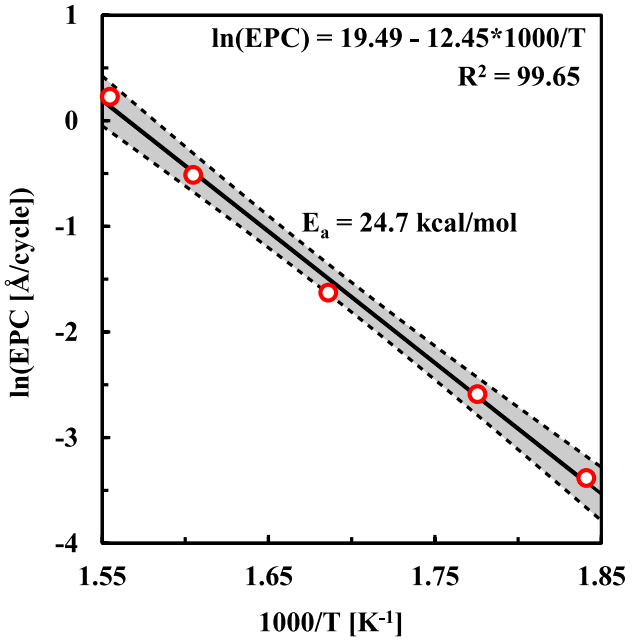


**Fig. 7.** Arrhenius plot of the temperature-dependent etch per cycle of TiN etching by $SOCl_2$.The shaded area is 95% confidence interval for the linear fit model with the $R^2$ of 99.65.

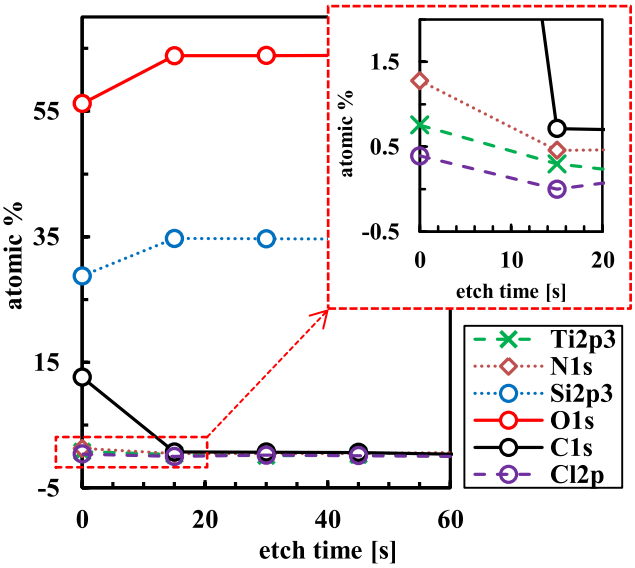


**Fig. 8.** An X-ray photoelectron spectroscopy of $SiO_2$ surface after complete removal of TiN film. Atomic percentages of different elements found on the surface are plotted at various etch times and the surface contaminants are shown in the zoomed-in picture at the top right corner.

be removed by additional etch cycles. $SOCl_2$ may also chlorinate the $SiO_2$ surface by forming stable Si-Cl bonds. However, the bulk of the silicon dioxide film shows no penetration of chlorine.

Fig. 9 is a cross-sectional bright field transmission electron microscope image of TiN coated 3D structures. The figure demonstrates partial as well as complete removal of about 4.4 nm thick TiN from non line-of-sight features. After partial removal of about 0.7 nm TiN, no significant increase in TiN film roughness is observed. Moreover, after complete removal of TiN from the $SiO_2$ substrate, the surface appears to be clean and devoid of significant surface remnants from the etch process.

Fig. 10 a) shows a reference pristine structure where about 22 nm

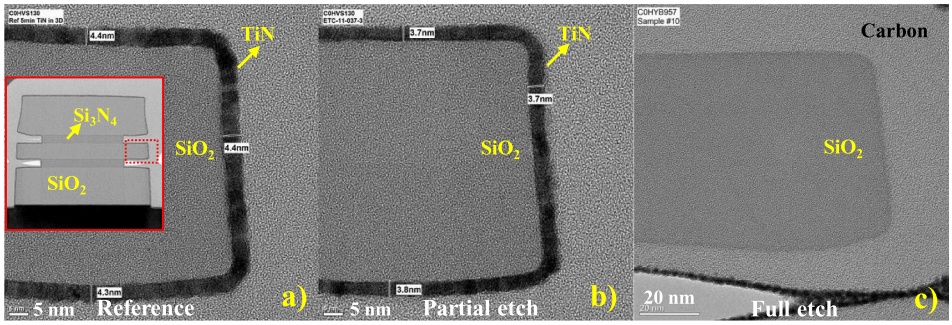


**Fig. 9.** Cross-sectional bright field transmission electron microscope (BF-TEM) images of TiN coated 3D structures. The inset is an image of patterned horizontal $SiO_2$ layers that are separated by $Si_3N_4$ layers and protruding out to form non line-of-sight features. The sub-figures depict; (a) highly conformal 4.4 nm TiN deposited on $SiO_2$, (b) the same after about 0.7 nm TiN is etched in 40 cycles, and (c) after complete removal of the 4.4 nm TiN film at the etch temperature of 320 °C.

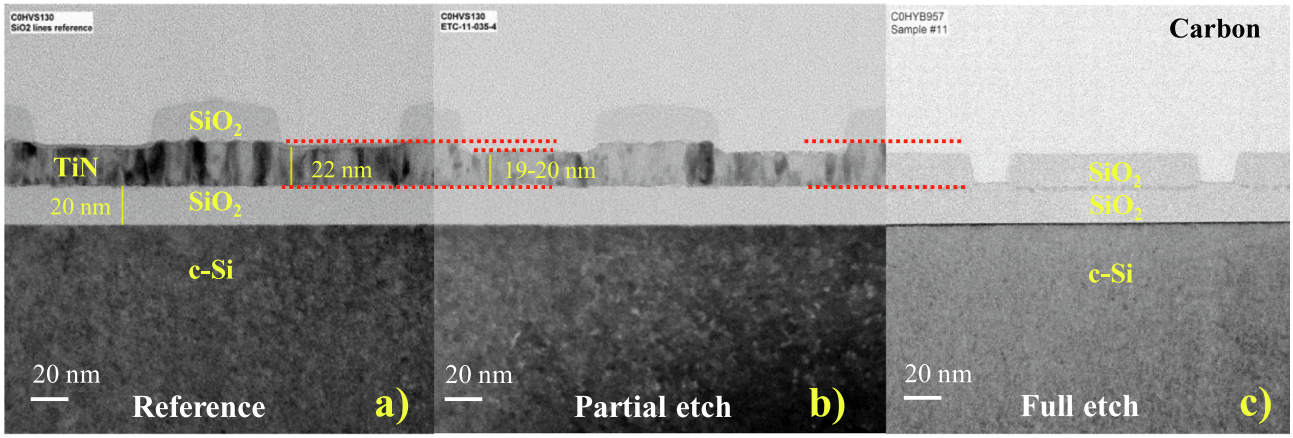


**Fig. 10.** Cross-sectional bright field transmission electron microscope (BF-TEM) images of; (a) patterned $SiO_2$ lines on about 22 nm TiN film, where a strong diffraction contrast is seen for the poly-crystalline TiN film, (b) the same after etching 2–3 nm of TiN, and (c) after complete isotropic removal of TiN underneath $SiO_2$ and thus consequent collapse of $SiO_2$ lines.

TiN film has been deposited on thermally grown $SiO_2$ layer, and on top of TiN, $SiO_2$ has been deposited by PECVD and the lines were patterned perpendicular to image plane. These structures were designed to study the isotropic nature of the etch process. In addition, the structure can also reveal etch selectivity of thionyl chloride towards $SiO_2$. From the figure it can be concluded that after removal of about 2–3 nm of TiN selectively over $SiO_2$, no significant increase in surface roughness is observed. A minor under-cut etch from the partially etched TiN surface can be seen as well. After employing over-etch the TiN is removed completely. Moreover, a full lateral etch that proceeded from both sides has resulted in a collapse of $SiO_2$ lines. Even after performing 1000 etch cycles at 370 °C, no etching of $SiO_2$ was seen, thus confirming the high selectivity. The long etch process may point towards an almost infinite selectivity against $SiO_2$ at 320 °C.

The images in Fig. 11 show surface roughness values ($R_a$) and morphology as obtained from the AFM. The measured surface roughness value for an unetched TiN is 0.54 nm. After removing about 7 nm TiN an increase in surface roughness to 0.81 nm is measured. Moreover, for the

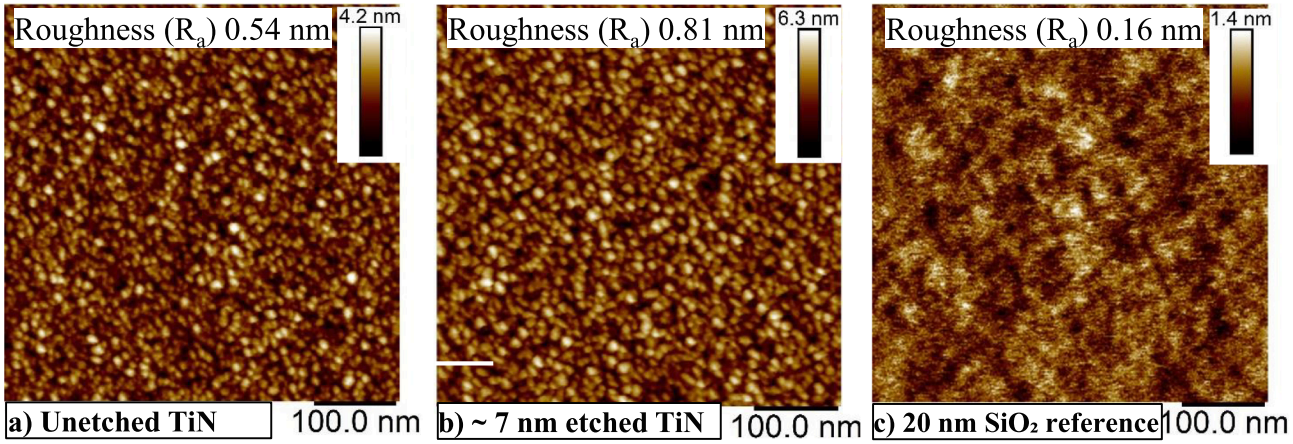


**Fig. 11.** Surface morphology and roughness by atomic force microscope of; (a) about 25 nm unetched TiN film on 20 nm $SiO_2$, (b) after etching about 7 nm of TiN, and (c) reference 20 nm $SiO_2$ film. The etch temperature was 320 °C.

etched TiN a slight increase in the grain size can be determined from the visual inspection. For comparison, the Fig. 11 c) shows the surface roughness value of 0.16 nm for 20 nm thermally grown silicon oxide. In contrast, the above TEM images (Fig. 9 and 10) do not show significant change in the surface roughness and this can be due to either the removal in a range of 0.5–3 nm only or imaging in different plane.

## 4. Conclusions

A successful demonstration of a gas-phase cyclic etching of TiN by $SOCl_2$ is reported. An EPC with sub-angstrom level precision can be achieved by applying gas-phase pulsed etching method. $SOCl_2$ is able to etch TiN at $T_{etch} \geqslant 270$ °C with a low EPC of about 0.03 Å at 270 °C increasing to 1.2 Å at 370 °C. Higher EPC at temperatures above 370 °C is anticipated, but not yet tested. From the Arrhenius plot an activation energy of 24.7 kcal/mol was determined.

From our findings, $SOCl_2$ is unable to etch $SiO_2$, $Si_3N_4$ and $Al_2O_3$ within the etch temperature range of 270 to 370 °C. The results are supported by thermodynamic calculations. For the $SOCl_2$-TiN etch system, many reactions showed a negative change in the enthalpy as well as the change in Gibbs free energy.

An XPS of $SiO_2$ surface after complete removal of titanium nitride films revealed no significant amount of residuals either from the etchant or the TiN films itself. From TEM analysis, an insignificant increase in the TiN surface roughness and high etch selectivity against $SiO_2$ was observed. However, the AFM image shows a small increase in the roughness for about 7 nm etched TiN surface.

## CRediT authorship contribution statement

**Varun Sharma:** Conceptualization, Investigation, Methodology, Software, Data curation, Writing - original draft, Visualization, Validation. **Tom Blomberg:** Conceptualization, Investigation, Supervision. **Suvi Haukka:** Supervision. **Shaun Cembella:** Investigation. **Michael E. Givens:** Writing - review & editing, Supervision. **Marko Tuominen:** Supervision. **Mikko Ritala:** Supervision.

## Declaration of Competing Interest

The authors declare that they have no known competing financial interests or personal relationships that could have appeared to influence the work reported in this paper.

## Acknowledgement

The authors thank Seastar chemicals ULC, Canada for supplying high purity $SOCl_2$ and Eurofins EAG Materials Science, LLC (California, USA) for TEM analysis.

## References

[1] P. Hammond, Chapter 25 - Vapor Phase Etch Processes for Silicon MEMS, in: Micro and Nano Technologies, William Andrew Publishing, Boston, 2015, pp. 540–549, https://doi.org/10.1016/B978-0-323-29965-7.00025-7.
[2] K.J. Kanarik, T. Lill, E.A. Hudson, S. Sriraman, S. Tan, J. Marks, V. Vahedi, R. A. Gottscho, Overview of atomic layer etching in the semiconductor industry, J. Vacuum Sci. Technol. A 33 (2) (2015) 020802, https://doi.org/10.1116/1.4913379.
[3] W.I. Jang, C.A. Choi, M.L. Lee, C.H. Jun, Y.T. Kim, Fabrication of MEMS devices by using anhydrous HF gas-phase etching with alcoholic vapor, J. Micromech. Microeng. 12 (3) (2002) 297–306, https://doi.org/10.1088/0960-1317/12/3/316.
[4] G.A. Rudakov, Gas-phase etching of SiO2 layers in an HF/C2H5OH mixture, Russ. Microlectron. 46 (2) (2017) 105–108, https://doi.org/10.1134/S1063739717010097.
[5] S.M. George, Y. Lee, Prospects for thermal atomic layer etching using sequential, self-limiting fluorination and ligand-exchange reactions, ACS Nano 10 (5) (2016) 4889–4894, https://doi.org/10.1021/acsnano.6b02991.
[6] S.M. George, Atomic layer deposition: An overview, Chem. Rev. 110 (1) (2010) 111–131, https://doi.org/10.1021/cr900056b.
[7] C. Fang, Y. Cao, D. Wu, A. Li, Thermal atomic layer etching: Mechanism, materials and prospects, Prog. Nat. Sci.: Mater. Int. 28 (6) (2018) 667–675, https://doi.org/10.1016/j.pnsc.2018.11.003.
[8] C.T. Carver, J.J. Plombon, P.E. Romero, S. Suriz, T.A. Tronic, R.B.T. Jr, Atomic layer etching: An industry perspective, ECS J. Solid State Sci. Technol. 4 (2) (2015) N5005–N5009, https://doi.org/10.1149/2.0021506jss.
[9] P.J. Holmes, J.E. Snell, A vapour etching technique for the photolithography of silicon dioxide, Microelectron. Reliab. 5 (4) (1966) 337–341, https://doi.org/10.1016/0026-2714(66)90162-4.
[10] X.-Q. Wang, X. Yang, K. Walsh, Y.-C. Tai, Gas-phase silicon etching with bromine trifluoride, in: Proceedings of International Solid State Sensors and Actuators Conference (Transducers '97), Vol. 2, 1997, pp. 1505–1508 vol 2. doi:10.1109/SENSOR.1997.635751.
[11] T. Kuijer, L. Giling, J. Bloem, Gas phase etching of silicon with HF, J. Cryst. Growth 22 (1) (1974) 29–33, https://doi.org/10.1016/0022-0248(74)90054-2.
[12] D.E. Ibbotson, J.A. Mucha, D.L. Flamm, J.M. Cook, Plasmaless dry etching of silicon with fluorine-containing compounds, J. Appl. Phys. 56 (10) (1984) 2939–2942, https://doi.org/10.1063/1.333834.
[13] G. Zhang, P. Qi, X. Wang, Y. Lu, X. Li, R. Tu, S. Bangsaruntip, D. Mann, L. Zhang, H. Dai, Selective etching of metallic carbon nanotubes by gas-phase reaction, Science 314 (5801) (2006) 974–977, https://doi.org/10.1126/science.1133781.
[14] H.F. Winters, J.W. Coburn, The etching of silicon with XeF2 vapor, Appl. Phys. Lett. 34 (1) (1979) 70–73, https://doi.org/10.1063/1.90562.
[15] N. Miki, H. Kikuyama, I. Kawanabe, M. Miyashita, T. Ohmi, Gas-phase selective etching of native oxide, IEEE Trans. Electron Devices 37 (1) (1990) 107–115, https://doi.org/10.1109/16.43806.
[16] D.B. Mawhinney, V. Naumenko, A. Kuznetsova, J.T. Yates, J. Liu, R.E. Smalley, Infrared spectral evidence for the etching of carbon nanotubes Ozone oxidation at 298 k, J. Am. Chem. Soc. 122 (10) (2000) 2383–2384, https://doi.org/10.1021/ja994094s.
[17] D. Kim, X. Yang, J. Woo, D. Um, C. Kim, Dry-etching properties of TiN for metal/high-k gate stack using BCl3 based inductively coupled plasmadoi:10.1116/1.3244567.
[18] R. Shul, C. Willison, M. Bridges, J. Han, J. Lee, S. Pearton, C. Abernathy, J. MacKenzie, S. Donovan, High-density plasma etch selectivity for the iii–v nitrides, Solid-State Electronics 42. doi:10.1016/s0038-1101(98)00224-x.
[19] N. Posseme, Plasma Etching Processes for CMOS Devices Realization, 1st Edition, ISTE Press - Elsevier, 2017.
[20] R. Hellriegel, M. Albert, B. Hintze, H. Winzig, J. Bartha, Remote plasma etching of titanium nitride using NF3/argon and chlorine mixtures for chamber clean applications, Microelectron. Eng., 84. doi:10.1016/j.mee.2006.08.002.
[21] F. Fracassi, R. d'Agostino, R. Lamendola, I. Mangieri, Dry etching of titanium nitride thin films in CF4-O2 plasmas, J. Vacuum Sci. Technol. A 13 (2) (1995) 335–342, https://doi.org/10.1116/1.579419.
[22] B. Jinnai, T. Nozawa, S. Samukawa, Damage mechanism in low-dielectric (low-k) films during plasma processes, J. Vacuum Sci. Technol. A: Microelectron. Nanometer Struct. Process., Meas. Phenom 26 (6) (2008) 1926–1932, https://doi.org/10.1116/1.3010721.
[23] G.Z. Yin, M. Ben-Dor, M.S. Chang, T.O. Yep, High-selectivity plasma etching of silicon dioxide on single-wafer etchers, J. Vacuum Sci. Technol. A 7 (3) (1989) 691–695, https://doi.org/10.1116/1.575867.
[24] Y. Karzhavin, W. Wu, Plasma induced charging and physical damage after dry etch processing, in: 1998 3rd International Symposium on Plasma Process-Induced Damage (Cat. No.98EX100), 1998, pp. 80–83.
[25] S.R. Min, H.N. Cho, Y.L. Li, S.K. Lim, S.P. Choi, C.W. Chung, Inductively coupled plasma reactive ion etching of titanium nitride thin films in a Cl2/Ar plasma, J. Industr. Eng. Chem., 14. doi:10.1016/j.jiec.2008.01.001.
[26] S.C. Abraham, Performance of different etch chemistries on titanium nitride antireflective coating layers and related selectivity and microloading improvements for submicron geometries obtained with a high-density metal etcher, J. Vacuum Sci. Technol. A Vacuum Surf. Films, 15. doi:10.1116/1.580805.
[27] K. Kolari, High etch selectivity for plasma etching SiO2 with AlN and Al2O3 masks, Microelectronic Engineering 85 (5) (2008) 985–987, proceedings of the Micro- and Nano-Engineering 2007 Conference. doi:10.1016/j.mee.2007.12.037.
[28] S.A. Vitale, J. Kedzierski, C.L. Keast, High density plasma etching of titanium nitride metal gate electrodes for fully depleted silicon-on-insulator subthreshold transistor integration, J. Vacuum Sci. Technol. B: Microelectron. Nanometer Struct. Process., Meas. Phenom 27 (6) (2009) 2472–2479, https://doi.org/10.1116/1.3253533.
[29] M. Darnon, T. Chevolleau, D. Eon, L. Vallier, J. Torres, O. Joubert, Etching characteristics of TiN used as hard mask in dielectric etch process, J. Vacuum Sci. Technol. B: Microelectron. Nanometer Struct. Process., Meas. Phenom 24 (5) (2006) 2262–2270, https://doi.org/10.1116/1.2338048.
[30] Y. Lee, S.M. George, Thermal atomic layer etching of titanium nitride using sequential, self-limiting reactions: Oxidation to TiO2 and fluorination to volatile TiF4, Chem. Mater. 29 (19) (2017) 8202–8210, https://doi.org/10.1021/acs.chemmater.7b02286.
[31] G. Dingemans, C.V. Helvoirt, M.V. de Sanden, W.M. Kessels, Plasma-assisted atomic layer deposition of low temperature SiO2, ECS Trans. 35 (4) (2011) 191–204, https://doi.org/10.1149/1.3572283.
[32] L. Gosset, J.-F. Damlencourt, O. Renault, D. Rouchon, P. Holliger, A. Ermolieff, I. Trimaille, J.-J. Ganem, F. Martin, M.-N.Séméria, Interface and material characterization of thin Al2O3 layers deposited by ALD using TMA/H2O, Journal of Non-Crystalline Solids 303. doi:10.1016/s0022-3093(02)00958-4.

[33] C.H. Ahn, S.G. Cho, H.J. Lee, K.H. Park, S.H. Jeong, Characteristics of TiCl4 thin films grown by ALD using TiCl4 and NH3, Metals and Materials International 7. doi:10.1007/bf03179261.
[34] D.R. Stull, Vapor pressure of pure substances. organic and inorganic compounds, Industr. Eng. Chem. 39 (4) (1947) 517–540, https://doi.org/10.1021/ie50448a022.
[35] M. Modreanu, P. Cosmin, S. Cosmin, C. Cobianu, C. Dunare, Measurement of CVD thin films thickness by sample weighing method, Vol. 2, 1996, IEEE 1996 International Semiconductor Conference. 19th Edition. doi:10.1109/smicnd.1996.557407.
[36] M.A. Greenbaum, J.A. Blauer, M.R. Arshadi, M. Farber, Heat of formation of AlOCl (g), Transactions of the Faraday Society 60. doi:10.1039/TF9646001592.
[37] J.T. Viola, D.W. Seegmiller, A.A. Fannin, L.A. King, Vapor pressure of aluminum chloride systems. 1. vapor pressure and triple point of pure aluminum chloride, J. Chem. Eng. Data 22 (4) (1977) 367–370, https://doi.org/10.1021/je60075a003.
[38] H.C. Lisel Bayer, Das aluminiumoxychlorid AlOCl, Zeitschrift für anorganische und allgemeine Chemie 263. doi:10.1002/zaac.19502630111.
[39] M. Farber, A.J. Darnell, The disproportionation and vapor pressure of TiCl3, J. Phys. Chem. 59 (2) (1955) 156–159, https://doi.org/10.1021/j150524a014.
[40] M. Farber, A.J. Darnell, F. Brown, X-ray diffraction patterns of TiCl2 and TiCl3, The Journal of Chemical Physics 23. doi:10.1063/1.1742366.
[41] G.B. Skinner, R.A. Ruehrwein, Thermodynamic properties of the titanium chlorides, J. Phys. Chem. 59 (2) (1955) 113–117, https://doi.org/10.1021/j150524a006.
[42] A. Okubora, J. Kasahara, M. Arai, N. Watanabe, Thermal etching of GaAs by hydrogen under arsenic overpressure, Journal of Applied Physics 60. doi:10.1063/1.337279.